bonyl group-containing 1,3-dioxolanes **2i** and **2j** were higher (93%) than that of *p*-toluenesulfonic acid.[1]

A few carbonyl compounds were also examined to the corresponding 5,5-dimethyl-1,3-dioxanes **4** with 2,2-dimethyl-1,3-propanediol in the presence of 1-3 mol% of **3**.

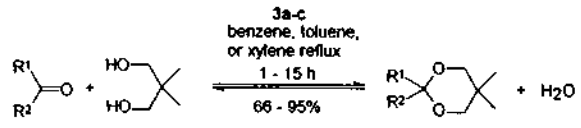

1a, d, f, g, h **4a, d, f, g, h**

1, 4	R^1	R^2	1, 4	R^1	R^2
a	Ph	H	g	Ph	Ph
d	-$(CH_2)_5$-		h	$MeOOCCH_2$	Me
f	Ph	Me			

Results shown in Table 2 demonstrate that **3b** effectively catalyzes the acetalization to give high yields of various 1,3-dioxanes **4** under the xylene reflux conditions.

Thus, a new class of acid catalysts for acetalization is developed which have high activities in the acetalization not only of arylketones but also of acid-sensitive carbonyl group-containing ketones. The significances of these catalysts are easy to use owing to their less hygroscopic nature and chemical stability toward air, water, and organic solvents.

References

1. Meskens, F. A. J. *Synthesis* **1981**, 501.
2. Sulzbacher, M.; Bergmann, E.; Pariser, E. R. *J. Am. Chem. Soc.* **1948**, *70*, 2827.
3. Salmi, E. J.; Kyrki, K. *Souom. Kemistil. B.* **1946**, *19*, 97. C. A. **1947**, *41*, 5480.
4. Sterzycki, R. *Synthesis* **1979**, 724.
5. Uno, H.; Endo, T. *J. Polym. Sci., Polym. Lett. Ed.* **1988**, *26*, 453.
6. Lee, S.-B.; Takata, T.; Endo, T. *Macromolecules* **1991**, *24*, 2693.
7. Uno, H.; Takata, T.; Endo, T. *Chem. Lett.* **1988**, 935.
8. Lee, S.-B.; Takata, T.; Endo, T. *Chem. Lett.* **1990**, 2019.
9. Lee, S.-B.; Lee, S.-D.; Takata, T.; Endo, T. *Synthesis* **1991**, 368.
10. Lee, S.-B.; Park, Y.-S.; Lee, K.-W.; Endo, T. *Chem. Lett.* **1995**, 287.
11. Wawzonek, S.; Yeakey, E. *J. Am. Chem. Soc.* **1960**, *82*, 5718.
12. Lee, S.-B.; Takata, T.; Endo, T. *Macromolecules* **1990**, *23*, 431.
13. Hamadzu, F.; Akashi, S.; Koizumi, T.; Takata, T.; Endo, T. *J. Polym. Sci., Polym. Chem.* **1991**, *29*, 1675.

Dynamics and Transport of Molecules Studied by Transient Grating Method: Methyl Red in Solution

Sun Hee Kim and Seong Kyu Kim*

Department of Chemistry, Sung Kyun Kwan University, Suwon 440-746, Korea
Received January 6, 1996

Time profile of the transient grating signal induced by a nanosecond pulsed laser excitation of methyl red is investigated in alcohols and toluene at several solvent temperatures. The signal decays biexponentially with well-separated time constants; the faster decay is identified as due to thermal diffusion of the solvents and the slower one as mainly due to translational diffusion of the solute. The measured translational diffusion constants of methyl red in toluene are close to a hydrodynamic prediction with a slip boundary condition while those in alcohols are larger by 30% and increase slightly with the size of alcohols. We compare the results with modified hydrodynamic models.

Introduction

Transient grating (TG) technique,[1] also known as laser-induced dynamic grating,[2] forced Rayleigh scattering,[3] holographic relaxation spectroscopy,[4] and many other names, is a sensitive method of measuring molecular relaxation and diffusion. The time scale that the TG technique covers is from femtoseconds to minutes. In the ultrashort time scale (shorter than a nanosecond),[4] the depopulation,[5,6] the vibrational dynamics,[7] the overall rotation,[6,8] the local structural relaxation,[9] the ultrasonic wave propagation,[10] the electron transfer,[11] etc in liquid or solid phases have been studied with state-of-the-art instrumentations of ultrafast lasers combined with precise control over optical and electronic timings. In the other extreme (slow) time scale, the TG method employs conventional instrumentations: cw lasers, a mechanical shutter and common detection electronics. The method probes mainly the translational diffusion of a dye in rigid hosts such as polymers,[12~14] liquid crystals,[15~17] or polymeric solutions.[18~20] The time resolution of such experiments is limited

*To whom correspondence should be addressed.

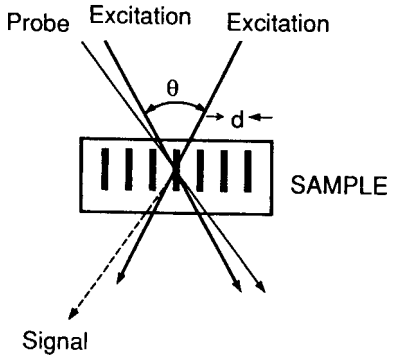

Scheme 1.

by the opening duration of the mechanical shutter for the laser excitation, that is some milliseconds.

In recent works by Terazima and coworkers,[21-23] a nanosecond pulsed laser has been employed for the TG to study the relaxation dynamics and the translational diffusion in solution, which occur in the time scale of microseconds to milliseconds. Many interesting measurements in the dynamics of photochromic molecules in solution were possible with the advantage of their short excitation pulse. Especially noteworthy but yet to be proved is the suggestion from their data that the translational diffusion of certain photogenerated radicals is several times slower than that of neutral counterparts.[22] This contrasts with a hydrodynamic picture and emphasizes specific interactions between the solute and the solvent. This suggests that microscopic friction models that take a solute-solvent interaction into account should be respected for predicting the diffusion of reaction intermediates. Because the lifetimes of the reaction intermediates are short, their diffusion rates are not measured readily by conventional techniques and should be predicted by a reliable microscopic model. In these respects, the importance of the TG technique is realized since it can provide accurate and systematic experimental data for the prediction of the translational diffusion.

We also expect that the TG technique with the nanosecond excitation can probe sensitively various solution phase relaxation dynamics which take place in the microsecond time scale. They may include the relaxations of photoinduced twisted state, charge transfer state, proton transfer state, and isomerized molecules. With these motivations, we have set up the TG experiments based on a nanosecond pulsed laser and have been studying systematically the molecular relaxation dynamics and diffusion in solution phase. We have selected methyl red in solution as the first test system since its *trans-cis* photoisomerization under a visible light is extensively studied and widely used as a photochromic probe in the TG experiments as well as in other nonlinear laser experiments. In the following few paragraphs, we will introduce briefly the methodology of the TG experiment and its application to methyl red system.

When two replica pulses of coherent laser light are overlapped spatially and temporally, a sinusoidal interference pattern of electric field forms. Once a sample that absorbs photons at the laser wavelength (λ_{ex}) is placed at the interaction region, a spatially modulated distribution of the excited and the unexcited molecules is created (Scheme 1) with a fringe

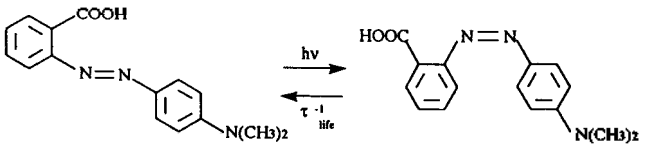

Scheme 2.

spacing d, given by

$$d=\frac{\lambda_{ex}}{2\ \sin(\theta/2)} \tag{1}$$

where θ is the crossing angle of the two excitation pulses.

The differences in the phase refractive index (Δn, defined as n_{bright}-n_{dark}) or the extinction coefficient (Δk, defined as k_{bright}-k_{dark}) between the excited and the unexcited molecules induce a transient grating which disappears through various relaxation processes. When a cw laser beam is introduced for probe into the interaction region, the transient grating diffracts a small fraction of the probe with the efficiency or the intensity of the diffracted signal ($I(t)$) being proportional to the square of the complex refractive index change.

$$I(t) \propto (\Delta n+i\Delta k)^2 \tag{2a}$$

$$=(\Delta n)^2+(\Delta k)^2 \tag{2b}$$

Methyl red exists in its *trans* form in the dark but converts to *cis* form under the illumination of wavelength shorter than ~590 nm (Scheme 2). The *trans*→*cis* photoisomerization involves the singlet $n\pi^*$ state, the triplet $\pi\pi^*$ state, the twisted phantom state.[24,25] The relaxations in these states and finally to the ground electronic states of the *trans* or the *cis* are mostly completed within a nanosecond. Then, the back conversion of the *cis* to the *trans* in the ground electronic state takes place in much longer time (τ_{life} in Scheme 2).

Since both *cis*- and *trans*-methyl red do not absorb photons at wavelengths longer than 590 nm, the Δk term in equation (2) can be neglected if a He-Ne laser is used for the probe. Therefore, only contributions of Δn to the diffracted signal are considered. In the time scale of nanoseconds and longer, the refractive index differences due to the thermal process (Δn_{th}) and the population relaxation (Δn_p) are the main contributions. That is,

$$I(t) \propto (\Delta n)^2=(\Delta n_{th}+\Delta n_p)^2 \tag{3}$$

The thermal grating (the contribution of Δn_{th}) is produced by the dissipation of excess energy from various molecular relaxation processes (e.g. internal conversion, vibrational relaxation, etc) into solvent thermal energy. Since the refractive index decrease with temperature, Δn_{th} is negative. It rises at the rate of the thermalization process and decays exponentially with a time constant of $\tau_{th}(=d^2/4\pi^2D_{th}$, where D_{th} is the thermal diffusion constant of solvent). The population grating (the contribution of Δn_p) rises at the rate of the *cis* formation and decays exponentially with a time constant τ_p. Both the depopulation time of the *cis* (τ_{life}) and the translational diffusion time of methyl red ($d^2/4\pi^2D$) are responsible for the decay of the population grating. That is

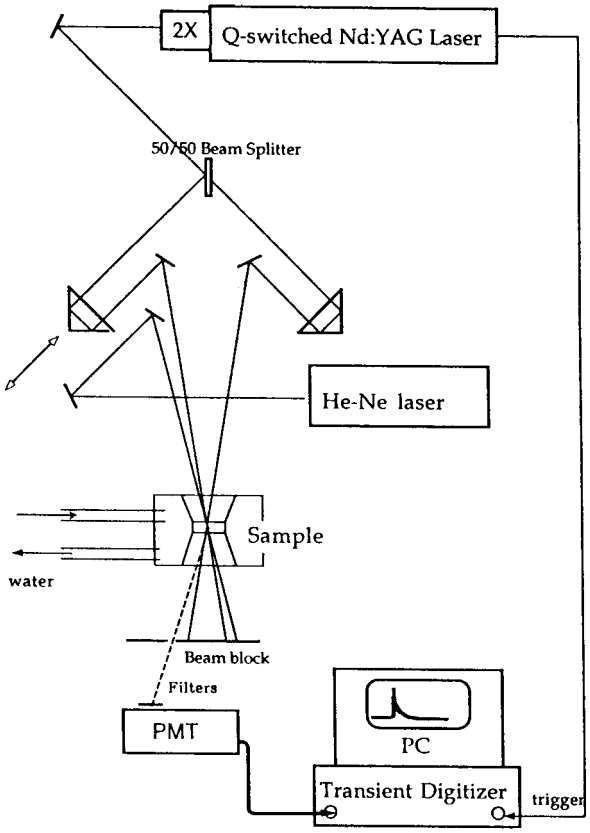

Figure 1. Optical layout of TG experiments.

$$\frac{1}{\tau_p}=\frac{1}{\tau_{life}}+\frac{4\pi^2 D}{d^2} \tag{4}$$

where D is the translational diffusion constant of methyl red. In our experimental condition, both the thermal and the population gratings rise instantaneously within the laser excitation. Therefore, $I(t)$ has the following form:

$$I(t)=[A_{th}\ \exp(-t/\tau_{th})+A_p\ \exp(-t/\tau_p)+B]^2+C \tag{5}$$

where the coherent background (B) and the incoherent background (C) are included for generalization.

Experimental

The optical layout of the TG experiment is shown in Figure 1. The 2nd harmonic (532 nm) pulse from a Q-switched Nd : YAG laser [Continuum, Surelite II] is split by half and recombined at the sample, creating the transient grating. We have not focused the laser beam but reduced the diameter of the beam at the sample to 3 mm by using apertures. The beam crossing angle can be varied between less than 1^0 and more than 10^0 and are measured accurately by projecting the beam over 1 meter away. The energy of the excitation pulse is about 1 mJ and the repetition rate is kept below 1 Hz. 5 mW of cw He-Ne laser (632.8 nm) is introduced for the probe at the Bragg angle. The polarizations of both the excitation and the probe are perpendicular to the laser table. The diffracted signal is spatially separated, colorly filtered, and attenuated before being detected by a photomultiplier tube [Hamamatsu, R928]. The signal voltage from the photomultiplier tube is then recorded by a 8 bit, 100 mega-sampling transient digitizer [Gagescope, CS250]. Typically, 100 transient signals are recorded and mathematically averaged. The background signals are also obtained by blocking one of the excitation beam, and then averaged and subtracted from the transient signal. We observed the photomultiplier tube signal deforms significantly due to the anode current overdrain when the outputs over 2 mV are to be fed into a 50 Ω termination. Therefore, we had to use a mismatched termination (1 KΩ) to withdraw enough output voltages for the transient digitizer. In sacrifice for it, the rise and the fall times of the signal become worse (but still tolerable) to 0.5 μs and 1 μs, respectively.

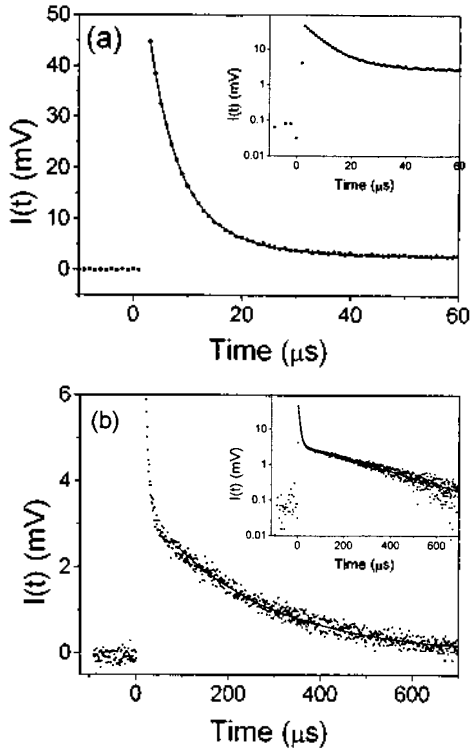

Figure 2. TG decay for methyl red in ethanol. The sample temperature was 50 ℃. The beam crossing angle was 5.8°. The early part of the decay is shown in (a) and the late part is shown in (b). Dot points are the experimental data and the solid lines are the best fit to the data. The data and the fit in semilogarithmic scale are shown in each inset. The fit function of (a) is $I(t)=[A_{fast}\ \exp(-t/\tau_{fast})+A_{slow}]^2$ with the fit parameters $A_{fast}=6.90$, $\tau_{fast}=9.60$ μs, $A_{slow}=1.64$, and that of (b) is $I(t)=[A_{slow}\ \exp(-t/\tau_{slow})]^2+C$ with the fit parameters $A_{slow}=1.90$, $\tau_{slow}=460$ μs, $C=7\times10^{-10}$.

Methyl red [Aldrich], the photochromic probe in this study, was used without further purification. Toluene [Samchun, GR grade] and alcohols [methanol, ethanol, 1-propanol, 2-propanol, 1-butanol, 1-hexanol, 1-octanol from Aldrich or Junsei] were the solvents and used after distillation over drying agents. About 1 mM of methyl red dissolved in each solvent was placed into a cuvette cell of 2 mm pathlength. The sample cell is held inside an aluminium block that is temperature controlled with a circulating water bath with an accuracy better than 1 ℃ in the range of 10-50 ℃.

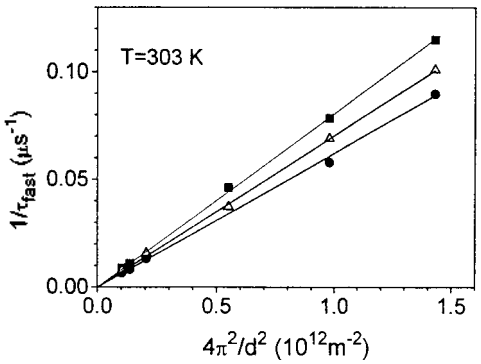

Figure 3. Plot of $1/\tau_{fast}$ versus $4\pi^2/d^2$ for toluene (■), 1-butanol (△), 2-propanol (●).

Table 1. Thermal diffusion constants of methyl red in various solvents as determined by the TG experiment in this work, by equation (7)† and by other experiments (in reference 23)

Solvent	D_{th} (in 10^{-8} m^2 s^{-1}) determined by		
	this work	equation (7)	reference 23
methanol	9.34	10.06	
ethanol	8.44	8.93	9.33
1-propanol	7.69	7.94	
1-butanol	7.05	7.77	
1-hexanol	6.40	8.55	
1-octanol	7.82	7.88	
2-propanol	6.17	6.81	7.81
toluene	8.07	8.90	

†: In applying equation (7), the solvent parameters λ_T, ρ, C_p are obtained from reference 28.

Results and Discussion

Characteristic time profile of TG signal. A typical decay profile of TG signal is shown in Figure 2. The TG signal in this particular example was obtained for methyl red dissolved in ethanol at the temperature of 50 ℃ and at the beam crossing angle of 5.8° (*i.e.* $d=5.3$ μm). The signal decays biexponentially with well-separated time constants. Therefore, we show the decay in the two time windows in Figure 2(a) and 2(b). The decay can be fitted to a function:

$$I(t)=[A_{fast}\ \exp(-t/\tau_{fast})+A_{slow}\ \exp(-t/\tau_{slow})]^2+C \quad (6)$$

where we include only the incoherent background C because we believe that under the experimental condition of a Q-switched laser forming the interference the incoherent background be more important than the coherent one. However, in most signals, the contributions of any background are found negligible and the inclusion of it into the fit function is mainly for precaution. The large difference in τ_{fast} and τ_{slow} makes it possible to fit the fast decay with $I(t)=[A_{fast}\ \exp(-t/\tau_{fast})+A_{slow}]^2$ and the slow decay with $I(t)=[A_{slow}\ \exp(-t/\tau_{slow})]^2+C$. The best fit decay times for Figure 2 are found as $\tau_{fast}=9.60$ μs and $\tau_{slow}=460$ μs.

Fast decay component. We have accumulated and analyzed the decays by varying the solvents, the solvent temperatures, and the beam crossing angles. The fast decay times are found less sensitive to the solvents or the solvent temperatures. When $1/\tau_{fast}$ are plotted versus $4\pi^2/d^2$, good linearities are found with no interceptions (Figure 3). These facts suggest that the thermal grating is responsible for the fast decay. That is, $\tau_{fast}=\tau_{th}$. Then, the slope of the plot $1/\tau_{th}$ versus $4\pi^2/d^2$ should give the thermal diffusion constant D_{th} of the solvent. In thermal diffusion theories, D_{th} is related to the density (ρ), the heat conductivity (λ_T), and the isobaric heat capacity (C_p) of solvent as in equation (7).[26]

$$D_{th}=\frac{\lambda_T}{\rho C_p} \quad (7)$$

The thermal diffusion constants of methyl red in various solvents determined by the TG experiment and by equation (7) are summarized in Table 1. The excellent agreement between the experimental and the theoretical values in Table 1 strongly supports the assignment of the fast decay component to the thermal grating.

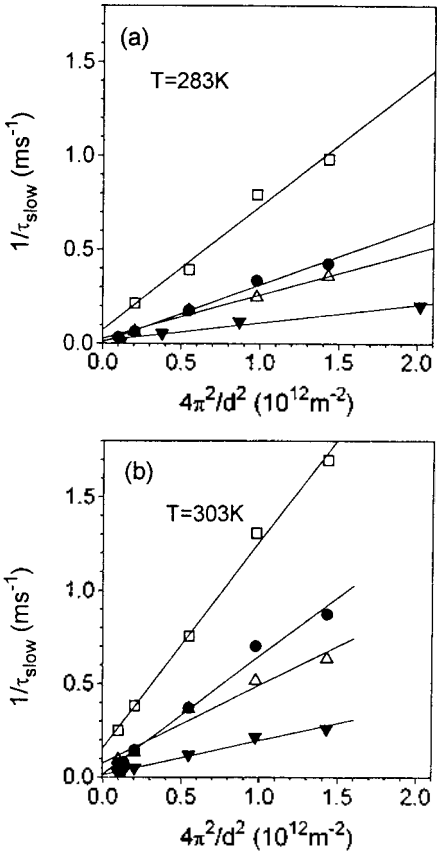

Figure 4. Plot of $1/\tau_{slow}$ versus $4\pi^2/d^2$ for ethanol (□), 2-propanol (●), 1-butanol (△), 1-octanol (▼) when the solvent temperatures are (a) 283 K and (b) 303 K.

Slow decay component. Figure 4 illustrates the plots of $1/\tau_{slow}$ versus $4\pi^2/d^2$ for several solvents and solvent temperatures. The slopes are sensitive to the solvents and the temperatures, and the intercepts show nonzero values. These suggest that the slow component of the decay be due to the population grating. Therefore, $\tau_{slow}=\tau_p$. According to

Table 2. The measured translational diffusion constants (in 10^{-9} m^2 s^{-1}) of methyl red in various solvents and at several solvent temperatures

Solvents	Temperatures				
	10.0 ℃	20.0 ℃	30.0 ℃	40.0 ℃	50.0 ℃
ethanol	0.692	0.688	1.11	1.20	1.44
1-propanol	0.371	0.467	0.670	0.720	0.870
1-butanol	0.231	0.310	0.420	0.600	0.720
1-hexanol	0.130	0.140	0.250	0.344	0.461
1-octanol	0.096	0.104	0.180	0.270	0.380
2-propanol	0.304	0.402	0.630	0.840	1.03
toluene	0.921	1.11	1.37	1.60	1.55

equation (4), the slope and the intercept should give the translational diffusion constant of methyl red (D) and the reciprocal time of the *cis*→*trans* isomerization ($1/\tau_{iso}$), respectively. In Table 2, we list only the D values determined from the slope.

The intercepts are unexpectedly large when considering the well-known relaxation time (an order of seconds) of the *cis*→*trans* isomerization. We considered three possibilities of experimental artifacts and have conducted several tests. The first possibility is that the intensity and the repetition rate of the excitation pulse are so high that during the data collection the accumulation of the *cis* may develop seriously and the transient grating may become inefficient as time goes by. This tends to shorten the decay times. However, when we attenuated the intensity of the excitation pulse or reduced the repetition rate, no apparent change in τ_{slow} was noticed. Besides, during the data accumulation the shape and efficiency of the TG signal do not change appreciably from the first to the last shot of the excitation pulses. The second possibility is that the high intensity of the probe laser (~5 mW) may open a different channel (possibly through the triplet state) of the *cis*→*trans* isomerization. As a matter of fact, there were reports that the TG decay for methyl red in liquid crystals[16(a)] or in polymer[13(d)] takes longer as the probe intensity is reduced. However, no such retardation is observed in our test of the probe attenuation. The third possibility is regarding experimental uncertainties in the measurements of the beam crossing angles or the solvent temperatures. The error in the time constant ($\Delta\tau$) due to the beam crossing angle uncertainty ($\Delta\theta$) is given by

$$\frac{\Delta\tau}{\tau} = \frac{\Delta\theta}{\tan(\theta/2)} \tag{8}$$

Therefore the degree of the error may become significant at small angles (*i.e.* at small values of $4\pi^2/d^2$). With the 0.5 mm uncertainty in measuring a projected interbeam spacing, $\Delta\tau/\tau$ is 0.05 when $\theta=1.56°$ and is 0.007 when $\theta=6.0°$. This error would result in a large uncertainty in the intercept of the plot but would affect little the slope since the values at larger angles are given higher weights in the least square analysis. The error due to the solvent temperature uncertainty (ΔT) is given by

Table 3. Activation energy of translational diffusion (E_a), activation energy of diffusion (E_η) for the solvents in this experiment, f determined from the plot of Figure 5, f_{SW} calculated with the Spernol-Wirtz model (equation (13) and (14))

Solvent	*E_a (kJ/mol)	*E_η (kJ/mol)	†f	‡f_{SW}
ethanol	15.4	15.0	0.424	0.44-0.46
1-propanol	16.3	17.7	0.418	0.45-0.48
1-butanol	22.3	19.2	0.413	0.43-0.45
1-hexanol	26.0	22.3	0.407	0.43-0.45
1-octanol	28.0	26.9	0.350	0.44-0.46
2-propanol	24.2	23.4	0.396	0.42-0.44
toluene	10.8	8.91	0.571	0.40-0.42

*: E_a is determined from ln D versus $1/T$ plot. E_η is determined from ln η versus $1/T$ plot. The solvent viscosities at various temperatures are obtained from references 28 and 33. †: In applying equations (11) and (12), the hydrodynamic radius of methyl red is estimated to be 5.50 Å. ‡: In applying equations (13) and (14), the radii of solvents are estimated from the density, the molecular weight and the free volume (74%) following reference 34, and the difference of boiling and freezing points of methyl red is assumed identical to that of azobenzene. The lower limit is for 10 ℃ and the upper limit is for 50 ℃.

$$\frac{\Delta\tau}{\tau} = \frac{E_a\Delta T}{RT^2} \tag{9}$$

where E_a is the activation energy of the decay process. The activation energy of the thermal diffusion is near zero and that of the translational diffusion is determined from the Arrhenius plot and listed in Table 3. Using the E_a values and estimating $\Delta T=1$ K, $\Delta\tau/\tau$ is calculated between 0.01 and 0.04. This experimental error induces negligible scattering in τ_{th} values and larger scattering in τ_p values as seen in Figures 3 and 4. Possibly, a combination of these three possibilities occurs simultaneously and makes the systematic tests difficult. At this point, we gave away identifying the unexpectedly fast relaxation times. Emphases are rather placed on interpreting the slope of the plot, which is presumably unaffected by the possibilities mentioned above.

A closer examination of the population decay in Figure 2(b) raises a question whether the single exponential function $I(t)=[A_{slow}\ \exp(-t/\tau_{slow})]^2+C$ fits the data perfectly. In other words, the semilogarithmic plot in the inset of Figure 2(b) shows a slightly downward curvature. This curvature results from two out-of-phase gratings that decay with different time constants: so-called a complementary grating effect.[27] In this case, the population grating is better described by

$$I(t)=[A_1\ \exp(-t/\tau_1)-A_2\ \exp(-t/\tau_2)]^2+C \tag{10a}$$

$$=[A_1\ \exp(-t/\tau_1)]^2\left(1-\frac{A_2}{A_1}e^{-\frac{(\tau_1-\tau_2)}{\tau_1\tau_2}t}\right)^2+C \tag{10b}$$

The factor $\left(1-\frac{A_2}{A_1}e^{-\frac{(\tau_1-\tau_2)}{\tau_1\tau_2}t}\right)^2$ in equation (10b) determines the curvature. When $\tau_1<\tau_2$ for $A_1>A_2$, there exists a positive

time $\left(t=\frac{\tau_1\tau_2}{\tau_2-\tau_1}\ln\frac{A_1}{A_2}\right)$ when the two out-of-phase gratings cancel each other completely and therefore a decay-rise-decay curve appears. When $\tau_1>\tau_2$ for $A_1>A_2$, such a cancellation time is negative, and therefore a downward curve appears. When $\tau_1=\tau_2$, equations (10a) and (10b) reduce to a single exponential. The population grating must be in phase with the thermal grating since the decay-rise-decay curve is not shown for $A_{th}>A_p$ and $\tau_{th}<\tau_p$. In other words, Δn_p is also negative.

The downward curvature appears in the data for the alcohol solvents but is absent for nonpolar solvents, as was pointed out by Terazima *et al.*[23] Since Δn_p is negative, the refractive index of the *cis* form must be smaller than the *trans* form and $A_{cis}<A_{trans}$. Therefore the diffusion of the *cis* must be faster than that of the *trans* ($\tau_{cis}<\tau_{trans}$) in alcohol solvents but is almost identical in nonpolar solvents. This explanation is plausible if the *trans* makes hydrogen bonding with alcohols more effectively than the *cis*. Park *et al.*[27] have simulated for the complementary grating effect, especially with optical parameters relevant to azobenzene. Following their analysis for our data, we estimate an upper limit of τ_{trans}-τ_{cis} to be 5% of the average in alcohols. Unfortunately, the accurate determination of τ_{trans} and τ_{cis} seems impossible with the signal-to-noise ratio of our data and we try to get the average value by fitting it with a single time constant.

Translational diffusion and hydrodynamic models. The translational diffusion constants determined from the slopes of $1/\tau_{slow}$ versus $4\pi^2/d^2$ plots are summarized in Table 2. For comparison, Terazima *et al.*[23] reported D of methyl red in room temperature ethanol and 2-propanol to be 0.90×10^{-9} m^2 s^{-1} and 0.56×10^{-9} m^2s^{-1}, respectively. In hydrodynamic models, the solute is assumed spherically shaped with a radius R and the solvent a continuum with the viscosity η. Then the translational diffusion constant is given by

$$D=\frac{kT}{\zeta} \tag{11}$$

with the solvent friction ζ given by

$$\zeta=6\pi\eta Rf \tag{12}$$

where f is a correction factor considering a solute-solvent boundary condition. In the original hydrodynamic model by Stokes and Einstein,[29] only the stick boundary condition is considered and $f_{stick}=1$. In the stick boundary condition, the normal components of velocity vectors for the solute and the solvent cancel each other while their tangential components conserve each other. However, the stick boundary condition holds for a large enough solute and an ignorable size solvent. For the solutes of molecular size, the slip boundary condition,[30] where the conservation of the tangential components of velocity is dependent on the solute shape, would be more adequate. In rotational diffusion, f_{slip} is zero for a sphere, f_{stick} for a needle, and well-tabulated for other spheroids.[31] In translational diffusion, the very rapid overall rotation approximates the solute to be a rough sphere. In this case $f_{slip}=2/3$.

The form of equations (11) and (12) provides the motivation to plot D versus T/η as shown in Figure 5 for some solvents. Linearities in the plots are found within a given

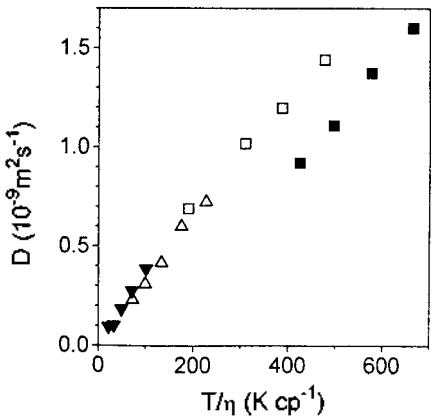

Figure 5. Plot of D versus T/η for various solvents : ethanol (□), 1-butanol (△), 1-octanol (▼), toluene (■).

solvent but the slopes vary from solvents to solvents. The slopes for the alcohol solvents are between 3.14×10^{-15} J m^{-1} K^{-1} (for ethanol) and 3.81×10^{-15} J m^{-1} K^{-1} (for 1-octanol) while increasing slightly with the size of the alcohols. The slope for nonpolar toluene is much smaller : 2.33×10^{-15} J m^{-1} K^{-1}. The trends that the diffusion rate versus T/η is linear in a given solvent but increases with the size of the solvent have been also observed in the rotational reorientation of *trans*-stilbene in normal alkane series[32(a)] and DODCI in normal alcohol series.[32(b)] In Table 3 we list the f values calculated by using the slopes and estimating the hydrodynamic radius of methyl red to be 5.50 Å. This value is the average radius of *trans*- and *cis*-methyl red along the longest molecular axis. The hydrodynamic radius is estimated along the longest molecular axis because rapid overall rotation displaces the solvent volume determined by the longest molecular axis. This may be valid when the overall rotation is faster than the collisional lifetime. Actually, the two time scales are comparable and therefore the solute radius and the f values are upper and lower limits, respectively. Anyhow, note that f value (0.57) for the nonpolar toluene solvent is close to f_{slip} (=2/3). The smaller f value than the theoretical one may be due to the overestimation of the hydrodynamic radius as explained above or by the microscopic friction effects as explained later. The averaged f value for the alcohol solvents is significantly smaller than that for toluene. This cannot be explained within the hydrodynamic picture because hydrodynamic radius of methyl red must be greater in the hydrogen bonding alcohol solvents. At this point, the lack of explicit expression in the hydrodynamic models overwhelms its merit in the simplicity of the model and the ready availability of macroscopic data. The explicit expression necessitates the microscopic friction models that take into account characteristics of solvents.

Microscopic friction models for translational diffusion. There have been microscopic friction models developed in two different ways : the quasi-hydrodynamic models and the kinetic models. In the quasi-hydrodynamic models, the simplicity of equations (11) and (12) is still taken with elaborated f. In a quasi-hydrodynamic model by Spernol and Wirtz,[34] effects of free volume created between finite sizes of solute and solvent are considered. Their semiempirical

f value is given by

$$f_{SW}=\left(0.16+0.4\frac{R_A}{r_B}\right)(0.3+0.4T_A'-0.25T_B') \quad (13)$$

where R_A and r_B are the radii of the solute and the solvent, respectively. T_A' and T_B' are the reduced temperatures calculated by

$$T_x'=\frac{(T-T_x^f)}{(T_x^b-T_x^f)} \quad (14)$$

where T_x^f and T_x^b are the freezing and the boiling points of the solute ($x=A$) and the solvent ($x=B$). The f_{SW} values calculated with the estimated molecular parameters are listed in Table 3. They seem to be in good agreement with the experimental ones for the alcohol solvents but are unacceptable for toluene. Most seriously, f_{SW} does not reflect the more sensitive dependence of f on the solvents themselves than the temperatures within a given solvent.

In contrast, the kinetic models generalize the solute-solvent boundary condition at the molecular level and have a potential to describe the microscopic friction better than the quasi-hydrodynamic models. However, the kinetic models have been developed for frictions induced by hard sphere collisions and thus need to extract molecular parameters approximated to hard sphere collision. Undesirably, the approximated molecular parameters would result in large uncertainties in the calculations. For this reason, we have not attempted to compare our experimental results with calculations based on the kinetic models but introduce them for qualitative comparison. The kinetic models starts with the diffusion constant defined by

$$D=\frac{kT}{\zeta}=(1/3)\int dt\langle \mathbf{v}\cdot\mathbf{v}(t)\rangle \quad (15)$$

where $\langle \mathbf{v}\cdot\mathbf{v}(t)\rangle$ is a time correlation function of solute velocity vectors that relaxes through various modes of collision. In the limit of uncorrelated collision (Enskog friction),[35]

$$\zeta_{EK}=\frac{4}{3}\pi\ \upsilon_r\ \sigma^2\ N\ g(\sigma)\ \mu \quad (16)$$

where μ is the solute-solvent reduced mass, $\upsilon_r=(8kT/\pi\mu)^{1/2}$ is the average relative thermal velocity, σ is the sum of the solute and the solvent hard sphere radii, N is the solvent number density, and $g(\sigma)$ is the contact value of the solute-solvent radial distribution function. The success of most microscopic kinetic models relies on the good evaluation of $g(\sigma)$, which requires an accurate intermolecular potential energy curve. For the hydrogen bonding methyl red-alcohol pairs the merit of the kinetic model is limited by the difficulty in getting reasonable intermolecular potential energy curve.

Evans and coworkers[36] considered the effects of other modes of collision (*i.e.* the correlated backscattering collision or the collective momentum feedback collision) and the modified friction is given by

$$\zeta_{Evans}=\zeta_{EK}-M\int_0^\infty dt\ R(t)\ \exp(-zt)|_{z=0} \quad (17)$$

where M is the mass of solute and the integral represents the Laplace transformation of the memory function $R(t)$ at its zero frequency ($z=0$). The evaluation of integral in equation (17) is complicated but ζ_{Evans} tends to overestimate the friction.[37]

In another modification of the microscopic friction, Hynes and coworkers[38] have generalized the boundary condition so that an inner-shell of solvent exists where the friction is microscopic while outside the shell the friction can be described hydrodynamically. According to their generalization,

$$D=D_{EK}+D_H \quad (18)$$

where D_{EK} is the microscopic Enskog diffusion constant ($D_{EK}=kT/\zeta_{EK}$) and D_H is the hydrodynamic diffusion constant of the subshell (the solute plus the inner shell of solvent). In other words,

$$D_H=\frac{kT}{6\pi\eta(R+r)f} \quad (19)$$

where R and r are radii of the solute and the solvent (or solvent shell), respectively. Equations (18) and (19) can be rewritten to show the deviations of the original hydrodynamic expression (equations (11) and (12)), that is

$$D/D_h=(D_{EK}/D_h)-(1+\gamma)^{-1}+1 \quad (20)$$

where D_h is the original hydrodynamic diffusion constant ($D_h=kT/6\pi\eta Rf$) and $\gamma=R/r$. The first term on the right side of equation (20) is the contribution of the Enskog diffusion to the deviation from the hydrodynamics and the second term represents the finite solvent molecule size correction (in D_H) to the original hydrodynamic value D_h. The third contribution of unity is the hydrodynamic prediction for D/D_h. In an analysis by Hynes and coworkers,[38] the first two contributions tend to cancel each other and D/D_h remains close to but slightly larger than unity as long as $\gamma>2$ and starts to increase (which implies the Enskog friction contributes more) as γ decreases below 2. The Hynes model emphasizes the level of the Enskog friction contribution depending on the solute-solvent size ratio. This trend in the Hynes' analysis agrees qualitatively with our experimental trend. Since alcohols makes hydrogen bonding in themselves the thickness of the solvent subshell is expected to be greater than that of toluene. Therefore γ for the alcohol solvents is smaller and the contribution of the Enskog diffusion constant increases.

Finally, we point out that the translational diffusion of methyl red in alcohols are faster than the self-diffusion of the solvents that have much smaller molecular sizes than that of methyl red. Also we noticed that, although not included in this work, the translational diffusion of methyl red dissolved in very viscous ethylene glycol is almost as fast as in much less viscous 1-propanol. Viscosities of the alcohols are much larger than those of alkanes of the similar size due to the hydrogen bonding network. The hydrogen bonding network can be locally broken in the vicinity of the solute. Therefore, the solute in alcohols may experience the reduced friction from the viscosity estimations. This can also be an explanation of the larger diffusion constants in alcohols than the hydrodynamic prediction.

Summary and Conclusions

In this study, we have demonstrated that the transient grating method can be used to study the molecular relaxation and the diffusion processes. When methyl red dissolved in

alcohols or in toluene is tested, the transient grating signal consists of two decaying components : the faster one due to thermal process and the slower one mostly due to the translational diffusion of methyl red. The translational diffusion constants obtained for alcohols are larger by 30% than predicted by the hydrodynamic model with a slip boundary condition, while those for toluene are much close. The reduced friction for the alcohol solvents cannot be explained within the hydrodynamic picture. The quasi-hydrodynamic model by Spernol and Wirtz can be formulated semiempirically considering free volume effects between the solute and the solvent but does not reflect the big difference in the reduced friction between alcohols and toluene. The microscopic friction models based on the kinetic hard sphere collision theory provide the right boundary condition at the molecular level but usage of them is limited by the uncertainty of the molecular parameters approximated to hard sphere collision. We note a modification by Hynes and coworkers[38] provides the generalized boundary condition not only at the molecular level but also at the macroscopic level and shows a qualitative explanation for the trend of our data.

Acknowledgment. This paper was supported by NON DIRECTED RESEARCH FUND (01 D 0540), Korea Research Foundation. We appreciate professors Terazima, Hongdoo Kim, Taihyun Chang for helpful discussions.

References

1. (a) Eichler, H. J.; Salje, G.; Stahl, H. *J. Appl. Phys.* **1973**, *44*, 5383. (b) Eichler, H. J. *Optica Acta* **1977**, *24*, 631.
2. Eichler, H. J.; Günter, P.; Pohl, D. W. *Laser-Induced Dynamic Gratings*; Springer-Verlag: Berlin, Heidelberg, New York; Tokyo, 1986.
3. Pohl, D. W.; Schwarz, S. E.; Irniger, V. *Phys. Rev. Lett.* **1973**, *31*, 32.
4. Fayer, M. D. *Ann. Rev. Phys. Chem.* **1982**, *33*, 63.
5. Myers, A. B.; Hochstrasser, R. M. *IEEE J. Quant. Electro.* **1986**, *QE-22*, 1482.
6. Phillion, D. W.; Kuizenga, D. J.; Siegman, A. E. *Appl. Phys. Lett.* **1975**, *27*, 85.
7. Tokmakoff, A.; Zimdars, D.; Sauter, B.; Francis, R. S.; Kwok, A. S.; Fayer, M. D. *J. Chem. Phys.* **1994**, *101*, 1741.
8. (a) Deeg, F. W.; Fayer, M. D. *J. Chem. Phys.* **1989**, *91*, 2269. (b) Stankus, J. J.; Torre, R.; Fayer, M. D. *J. Phys. Chem.* **1993**, *97*, 9478. (c) Eyring, G.; Fayer, M. D. *J. Chem. Phys.* **1984**, *81*, 4314. (d) Moog, R. S.; Ediger, M. D.; Boxer, S. G.; Fayer, M. D. *J. Phys. Chem.* **1982**, *86*, 4694.
9. (a) Silence, S. M.; Duggal, A. R.; Dhar, L.; Nelson, K. A. *J. Chem. Phys.* **1992**, *96*, 5448. (b) Sengupta, A.; Terazima, M.; Fayer, M. D. *J. Phys. Chem.* **1992**, *96*, 8619.
10. (a) Marshall, C. D.; Fishman, I. M.; Fayer, M. D. *Phys. Rev. B*, **1991**, *43*, 2696. (b) Meth, J. S.; Marshall, C. D.; Fayer, M. D. *J. Appl. Phys.* **1990**, *67*, 3362. (c) Dwayne Miller, R. J.; Casalegno, R.; Nelson, K. A.; Fayer, M. D. *Chem. Phys.* **1982**, *72*, 371. (d) Nelson, K. A.; Fayer, M. D. *J. Chem. Phys.* **1980**, *72*, 5202.
11. (a) Kasinski, J. J.; Gomez-Jahn, L. A.; Faran, K. J.; Gracewski, S. M.; Dwayne Miller, R. J. *J. Chem. Phys.* **1989**, *90*, 1253. (b) Dorfman, R. C.; Lin, Y.; Zimmt, M. B.; Baumann, J.; Domingue, R. P.; Fayer, M. D. *J. Phys. Chem.* **1988**, *92*, 4258.
12. Todorov, T.; Nikolova, L.; Tomova, N.; Dragostinova, V. *IEEE J. Quant. Electro.* **1986**, *QE-22*, 1262.
13. (a) Wang, C. H.; Xia, J. L. *J. Phys. Chem.* **1992**, *96*, 190. (b) Wang, C. H.; Xia, J. L. *J. Chem. Phys.* **1990**, *92*, 2603. (c) Xia, J. L.; Wang, C. H. *J. Chem. Phys.* **1988**, *88*, 5211. (d) Gong, S. S.; Christensen, D.; Zhang, J.; Wang, C. H. *J. Phys. Chem.* **1987**, *91*, 4504. (e) Zhang, J.; Wang, C. H. *Macromolecules* **1987**, *20*, 2296. (f) Zhang, J.; Yu, B. K.; Wang, C. H. *J. Phys. Chem.* **1986**, *90*, 1299. (g) Zhang, J.; Wang, C. H.; Chen, Z.-X. *J. Chem. Phys.* **1986**, *85*, 5359.
14. (a) Sung, J.; Chang, T. *Polymer* **1993**, *34*, 3741. (b) Lee, J.; Park, K.; Chang, T.; Jung, J. C. *Macromolecules* **1992**, *25*, 6977.
15. Wiesner, U.; Antonietti, M.; Boeffel, C.; Spiess, H. W. *Makromol. Chem.* **1990**, *191*, 2133.
16. (a) Urbach, W.; Hervet, H.; Rondelez, F. *J. Chem. Phys.* **1985**, *83*, 1877. (b) Hervet, H.; Urbach, W.; Rondelez, F. *J. Chem. Phys.* **1978**, *68*, 2725.
17. Wesson, J. A.; Takezoe, H.; Yu, H.; Chen, S. P. *J. Appl. Phys.* **1982**, *53*, 6513.
18. Léger, L.; Hervet, H.; Rondelez, F. *Macromolecules* **1981**, *14*, 1732.
19. (a) Lee, J.; Kim, H.; Yu, H. *Macromolecules* **1988**, *21*, 858. (b) Kim, H.; Chang, T.; Yohanan, J. M.; Wang, L.; Yu, H. *Macromolecules* **1986**, *19*, 2737.
20. Lee, J.; Park, T.; Sung, J.; Park, S.; Chang, T. *Bull. Korean Chem. Soc.* **1991**, *12*, 569.
21. (a) Terazima, M. *Chem. Phys. Lett.* **1994**, *218*, 574. (b) Terazima, M.; Hirota, N. *J. Chem. Phys.* **1991**, *95*, 64 90.
22. (a) Terazima, M.; Okamoto, K.; Hirota, N. *J. Chem. Phys.* **1995**, *102*, 2506. (b) Terazima, M.; Okamoto, K.; Hirota, N. *J. Phys. Chem.* **1993**, *97*, 13387. (c) Terazima, M.; Hirota, N. *J. Chem. Phys.* **1993**, *98*, 6257.
23. (a) Terazima, M.; Okamoto, K.; Hirota, N. *Laser Chem.* **1994**, *13*, 169. (b) Terazima, M.; Okamoto, K.; Hirota, N. *J. Phys. Chem.* **1993**, *97*, 5188.
24. Ross, D. L.; Blanc, J. In *Photochromism*; Brown, G.H., Ed.; Wiley: New York, U.S.A., 1972; Ch. 5.
25. Griffiths, J. *J. Chem. Soc. Rev.* **1972**, *1*, 481.
26. Tyrrell, H. J. V. *Diffusion and Heat Flow in Liquids*; Butterworth: London, U.K., 1961.
27. Park, S.; Sung, J.; Kim, H.; Chang, T. *J. Phys. Chem.* **1991**, *95*, 7121.
28. (a) Dean, J. A. *Lange's Handbook of Chemistry*, 14th ed.; McGraw-Hill: New York, U.S.A., 1992. (b) Lide, D. R. *CRC Handbook of Chemistry and Physics*, 71st ed.; CRC press: Boca Raton; Ann Arbor; Boston, 1990.
29. Einstein, A. *Investigations on the Theory of Brownian Motion*; Dover: New York, 1956.
30. Zwanzig, R.; Bixon, M. *Phys. Rev. A* **1970**, *2*, 2005.
31. Hu, C.-M.; Zwanzig, R. *J. Chem. Phys.* **1974**, *60*, 4354.
32. (a) Kim, S. K.; Fleming, G. R. *J. Phys. Chem.* **1988**, *92*, 2168. (b) Waldeck, D. H.; Fleming, G. R. *J. Phys. Chem.* **1981**, *85*, 2614.
33. *Landolt-Börnstein*; New Series II/5; Springer Verlag: Berlin; Heidelberg; New York, 1967.
34. Spernol, A.; Wirtz, K. *Z. Naturforsh. A* **1953**, *8*, 522.
35. Chandler, D. *J. Chem. Phys.* **1974**, *60*, 3500.

36. (a) Kumar, B.; Evans, G. T. *J. Chem. Phys.* **1989**, *90*, 1812.
(b) Evans, G. T. *J. Chem. Phys.* **1988**, *88*, 5035.
37. Ravi, R.; Ben-Amotz, D. *Chem. Phys.* **1994**, *183*, 385.
38. Hynes, J. T.; Kapral, R.; Weinberg, M. *J. Chem. Phys.* **1979**, *70*, 1456.

Polymerization of Methyl Methacrylate with Phenylsilane

Hee-Gweon Woo*, Sun-Hee Park, Jin-Young Park, Soo-Yeon Yang, Heui-Suk Ham, and Whan-Gi Kim†

Department of Chemistry, Chonnam National University, Kwangju 500-757, Korea
†Samyang Group R&D Center, Taejon 305-348, Korea
Received January 8, 1996

The bulk thermal and photopolymerization of methyl methacrylate (MMA) with phenylsilane were performed to produce poly(MMA)s containing phenylsilyl moiety presumably as an end group. It was found for both thermal and photopolymerization that while the polymerization yields and polymer molecular weights decreased as the relative phenylsilane concentration increases, the TGA residue yields and the relative intensities of SiH IR stretching bands increased with increasing molar ratio of phenylsilane over MMA. The polymerization yield, molecular weight, and TGA residue yield for the thermal polymerization were higher than those for the photopolymerization. Thus, the phenylsilane seemed to significantly influence on the polymerization as both chain initiation and chain transfer agents. However, an appreciable silane effect was not observed on the thermal and photopolymerization of 4-vinylpyridine, acrylonitrile, styrene, and vinyltrimethoxysilane.

Introduction

A wide variety of unsaturated vinyl derivatives can be induced to undergo free-radical chain polymerization.[1] The capability to carry out a thermodynamically feasible polymerization relys on its kinetic feasibility on whether the process proceeds at a reasonable rate under a given set of reaction conditions. Initiator or promotor are often required to achieve the kinetic feasibility. Photopolymerization technology applicable conveniently is widely employed on a commercial scale today in the areas of surface coatings, photoresists, adhesives, and holography.[1] Although any vinyl monomer that will undergo chain polymerization is basically subject to photopolymerization or photosensitized polymerization, only a few unsaturated monomers are known to absorb 250-500 nm wavelength light which is the most convenient wavelength range for experimental work. The detailed mechanism of the formation of the propagating radicals in this case is not throughly understood, but it appears to involve the conversion of an electronically excited singlet state of the monomer to a long-lived excited triplet state.[2]

Hydrosilane is known to participate in versatile reactions such as free radical reduction of organic halides,[3] nucleophilic reduction of carbonyl compounds,[4] dehydropolymerization,[5] cross-dehydrocoupling,[6] and hydrosilation of olefins[7] with catalyst. The hydrosilation has been used to prepare many intriguing types of silicon containing polymers such as dendrimers[8] and copolymers.[9] We reported the bulk photopolymerization of methyl methacrylate (MMA) with various silanes.[10] Here we wish to report the bulk thermal and photopolymerization of MMA with phenylsilane to give poly (MMA)s containing phenylsilyl moiety presumably as an end group. We also describe the silane effect on the bulk thermal and photopolymerization of various vinyl derivatives.

Experimental Section

Materials and Instrumentation. All reactions and manipulations were performed under prepurified nitrogen using Schlenk techniques. Dry, oxygen-free solvents were employed throughout. Glassware was flame-dried or oven-dried before use. Infrared spectra were obtained under the same conditions such as cell thickness, sample concentration, etc. using a Nicolet 520P FT-IR spectrometer. Proton NMR spectra were recorded on a Bruker ASX 32 (300 MHz) spectrometer using $CDCl_3/CHCl_3$ as a reference at 7.24 ppm downfield from TMS. Gel permeation chromatography (GPC) was carried out on a Waters Millipore GPC liquid chromatograph. The calibrant (monodisperse polystyrene) and the sample were dissolved in THF and separately eluted from an Ultrastyragel GPC column series (sequence 10^3, 10^4, 10^5, 10^6 Å columns). Molecular weights were extrapolated from the calibration curve derived from the polystyrene standard. Data analyses were carried out using a Waters Data Module 570. Thermogravimetric analysis (TGA) of polymer sample was performed on a Perkin Elmer 7 Series thermal analysis system under a nitrogen flow (50 mL/min). The polymer sample was heated from 25 to 700 ℃ at a rate of 10 ℃/min. TGA residue yield (as a matter of convenience, read at 400 ℃) is reported as the percentage of the sample remaining after completion of the heating cycle. For the photolysis experiments a Raynot photochemical reactor (model RPR-2080) made